Vol. 36, No. 1
April 2018

JOURNAL OF
RADIATION
EFFECTS
Research and Engineering

Verification and Validation of MCNP6.1 Neutron Protection Factor Estimates of an Armored Vehicle Surrogate Using the White Sands Missile Range Fast Burst Reactor

A.W. Decker, S.A. Heider, M. Millett, S.R. McHale, J.A. Clinton, and J.W. McClory

This paper was presented at the 34th Annual HEART Technical Interchange Meeting
Denver, CO, April 24 – 28, 2017.

Prepared by AECOM for the HEART Society under contract to NSWC Crane

This work was sponsored by the Defense Threat Reduction Agency. The views in this article are those of the authors and do not reflect the official policy or position of the United States Army, Air Force, Department of Defense, or Government.

JOURNAL OF RADIATION EFFECTS,
Research and Engineering
Vol. 36, No. 1, April 2018

VERIFICATION AND VALIDATION OF MCNP6.1 NEUTRON PROTECTION FACTOR ESTIMATES OF AN ARMORED VEHICLE SURROGATE USING THE WHITE SANDS MISSILE RANGE FAST BURST REACTOR

A.W. Decker and S.A. Heider
Defense Threat Reduction Agency
West Point, NY

M. Millett and S.R. McHale
United States Naval Academy
Annapolis, MD

J.A. Clinton and J.W. McClory
Air Force Institute of Technology
Wright-Patterson AFB, OH

Abstract

Building upon past successful verification and validation (V&V) efforts for MCNP6.1-derived radiation protection factor (RPF) estimates, this experiment sought to V&V MCNP6.1-estimated neutron protection factor (NPF) values for an armored vehicle surrogate when exposed to a ^{235}U fission spectrum at a horizontal distance of 12 ft. The neutron source for both the experimental and computational analyses was the White Sands Missile Range Fast Burst Reactor. Neutron fluxes for both shielded and unshielded configurations were measured using a Bonner sphere spectrometer and LiI(Eu) scintillator, and the spectra were unfolded using MAXED, a maximum entropy deconvolution code. The computed neutron spectra for both configurations were likewise tallied by MCNP6.1, and both computational and experimental neutron flux results were converted to total ambient dose equivalent (H(10)). The dose values facilitated NPF calculations for the armored surrogate, which were experimentally-determined to be 1.22 ± 0.06, while MCNP6.1 estimated a value of 1.18 ± 0.02. This NPF value agreement strongly supports the V&V and eventual accreditation of MCNP6.1 for radiation protection factor assessments of military vehicles.*

Introduction

Since the Cold War, U.S. military vehicle ballistic shielding has improved significantly; however, the degree of protection that modern military vehicles provide against ionizing radiation remains uncertain. In March 2011, this shortfall became evident during Operation Tomodachi when radiation protection information about military vehicles was requested by, but unavailable to, operational decision-makers [1]. Furthermore, due to mounting risk of a conventional or unconventional nuclear attack in the world, the U.S. military will likely be forced to operate on a nuclear battlefield. In either case, the detailed knowledge of how well U.S. military vehicles protect their occupants from radiation cannot be overvalued, and the current inability of the U.S. military to provide this information demands attention.

To address this gap, the Defense Threat Reduction Agency (DTRA) and the U.S. Army Nuclear and Combating Weapons of Mass Destruction Agency (USANCA) partnered in 2014 to establish a multi-year plan to quantify radiation protection factors (RPF) for modern U.S. military vehicles. Due to the costs and limitations associated with physical experimentation, DTRA recognized comprehensive RPF analyses could only be achieved through the verification and validation (V&V) of a computational tool.

This work was sponsored by the Defense Threat Reduction Agency. The views in this article are those of the authors and do not reflect the official policy or position of the United States Army, Air Force, Department of Defense, or Government.

To that end, a Monte-Carlo transport code, MCNP6.1, was selected and DTRA began evaluations of the code for that purpose. Historically, Army researchers would conduct V&V of computer codes by evaluating experimental measurements using simplified surrogate vehicles and comparing those results against code predictions [2]–[4]. The current approach to V&V MCNP6.1 mirrors those benchmark methodologies, and examinations to this point have proven successful [5]–[10].

Here we report recent experimental and computational RPF results for an armored vehicle surrogate when subjected to short-duration neutron fluxes from the Fast Burst Reactor (FBR) at White Sands Missile Range (WSMR). This research directly supports the larger effort to V&V MCNP6.1, and through these combined analyses, DTRA aims to provide the most cost-efficient and reliable method for estimating RPF values of current U.S. military vehicles.

Theory

Protection Factors

The degree of protection that any material, vehicle, structure, etc. provides against the potentially harmful effects of radiation can be quantified by its radiation protection factor (RPF), defined as

$$\text{RPF}=\frac{\text{Unshielded Dose (n + γ)}}{\text{Shielded Dose (n + γ)}}. \quad (1)$$

RPF values account for dose contributions from both neutrons (n) and gamma rays (γ), and one crucial component of the RPF is the neutron protection factor (NPF), which quantifies only the protection offered by a shielding medium against neutrons. The NPF is calculated as

$$\text{NPF}=\frac{\text{Unshielded Dose due to Neutrons}}{\text{Shielded Dose due to Neutrons}}, \quad (2)$$

which is the subject of the work reported here. Note that in both (1) and (2), a greater value of protection factor implies more effective shielding.

Bonner Sphere Spectrometer

The Bonner Sphere Spectrometer (BSS) was first introduced in 1960 to measure neutron energy spectra [11]. A BSS consists of polyethylene spheres of various sizes, typically paired with a small (4mm × 4mm) LiI(Eu) scintillator crystal. The scintillator is inserted into the center of each sphere during measurements, and the ^{6}Li within the crystal offers a relatively large thermal neutron absorption cross section of 838 barns [12]. Each neutron absorption releases a total energy of 4.78 MeV, in the reaction

$$^{1}_{0}\text{n} + {}^{6}_{3}\text{Li} \rightarrow {}^{3}_{1}\text{H (2.73 MeV)} + {}^{4}_{2}\text{He (2.05 MeV)}. \quad (3)$$

The large ratio between the scattering and absorption cross section for polyethylene maximizes the likelihood that incident neutrons will become thermalized before reaching the LiI(Eu) crystal [13], as shown in Fig. 1.

Exchanging polyethylene spheres between neutron flux measurements allows the scintillator to record neutron response for each specific radius of moderator material. Typical experiments include measurements with the bare scintillator, as well as the 2-, 3-, 5-, 8-, 10-, and 12-inch diameter polyethylene Bonner spheres. As the radius of the moderating sphere increases, the scintillator responds more noticeably to higher energy neutrons because fast neutrons are more likely than lower-energy neutrons to survive parasitic capture and reach the scintillator.

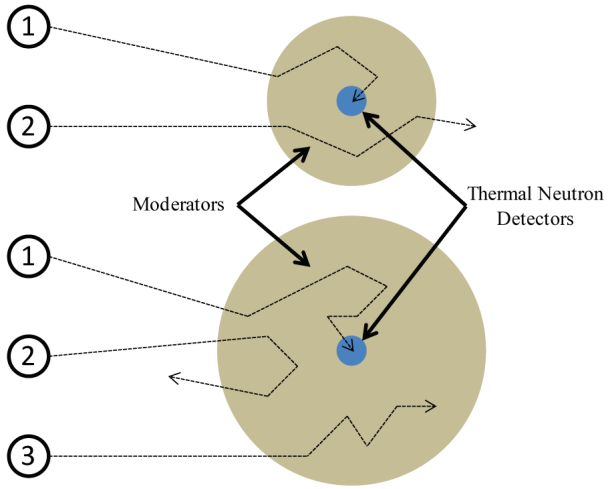

Figure 1. Schematic of possible neutron tracks within two Bonner spheres of different sizes. Track 1 represents neutrons moderated by the polyethylene and detected by the crystal, Track 2 represents partially-moderated neutrons that escape, and Track 3 shows how neutrons may suffer parasitic capture within the moderator material. Larger spheres tend to enhance the frequency of Track 3, while reducing the frequency of Track 2 (adapted from [14], p. 554).

The spectral energy distribution of the incident neutron field is deduced in a process called spectrum unfolding and requires a known BSS response matrix, which couples pulse height and energy intervals across their simulated domains. This work utilized a BSS response matrix calculated via MCNP6 simulations of a LiI(Eu) scintillator exposed to neutrons in 26 discrete energy groups, as described elsewhere [6].

Finally, it should be noted that the BSS inherently suffers from relatively poor detector resolution across intermediate energy ranges (10 eV – 100 keV) due to the lack of strong structures across that region of the response matrix [15].

MAXED

Spectra unfolding was accomplished using the Maximum Entropy Deconvolution (MAXED) algorithm. MAXED calculates an optimal neutron flux solution based on measured BSS count rates, an *a priori* spectrum, and the provided response matrix [16].

Using the entropy equation,

$$S = -\sum\left(f_i \ln\left(\frac{f_i}{f^{DEF}} \right) + f^{DEF} - f_i \right), \qquad (4)$$

MAXED seeks to identify the solution spectrum, f_i, using the default (or *a priori*) spectrum, f^{DEF}, which maximizes the entropy, *S*. This provides a solution spectrum that most closely matches the *a priori* information and also adheres to the experimentally determined count rates and uncertainties. MAXED solves the resulting Lagrangian in terms of the first multiplier, λ_k, which provides a set of *m* equations with *m* unknowns, $\lambda_1 \ldots \lambda_m$. Each solution spectrum provided by MAXED is evaluated using an associated χ^2/df value, with a value less than one indicating a statistically significant solution [16].

Experiment

The purpose of this research was to further the V&V of MCNP6.1-generated NPF estimates by extending prior work that used a simplified vehicle surrogate shielded on all sides by 2.54 cm of steel [8]. New investigations reported here employed a surrogate vehicle shielded with basic ballistic armor more representative of that found on U.S. military vehicles. This new surrogate consisted of a box with side lengths of 62.27 cm and 3.175 cm thick walls, composed of material layers (from inside to out) of 1.27 cm steel, 1.27 cm glass reinforced plastic (GRP), and 0.635 cm aluminum, which represented the vehicle frame, anti-spallation liner, and skin, respectively. The ^{235}U fission neutron spectrum for this experiment was generated by the FBR located at WSMR.

Experimental Design

An armored vehicle surrogate was used, consistent with the legacy radiation transport experiments using similar surrogates constructed of iron or steel [2], [5]. The material plates were bolted to an internal frame, as depicted in Fig. 2, made of aluminum due its low microscopic cross section for fast and epithermal neutron absorption. The three-inch diameter hole at the top of Fig. 2 allowed for the insertion of the LiI(Eu) scintillator and photomultiplier tube into the polyethylene Bonner spheres, as required to measure the response of the shielded spectrometer within the armored vehicle surrogate. For unshielded measurements, the surrogate was simply removed.

In both experimental configurations, aluminum stability rings and an aluminum laboratory jack ensured consistent positioning and orientation of the scintillation crystal across all measurements. For every measurement, the LiI(Eu) scintillator was positioned at a horizontal distance of exactly 12 ft from the middle of the FBR and centered on it vertically.

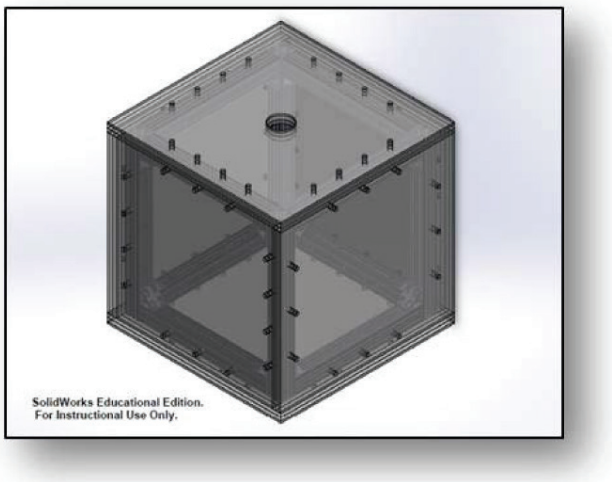

Figure 2. Schematic of the armored vehicle surrogate testing apparatus, shown with the scintillator opening in the upward position. The three armor layers are bolted to an aluminum frame during shielded measurements.

The absolute BSS count rates were recorded via Ortec Maestro software and associated uncertainties for both the shielded and unshielded configurations were input into the MAXED software, which unfolded the experimental solution spectra. Spectra were then normalized to facilitate comparison against the computational neutron flux spectra data.

Computational Design

The experimental geometry was replicated in MCNP6.1, including the armored vehicle surrogate. A depiction of the input file geometry is shown in Fig. 3 for the shielded configuration.

The FBR was modeled as a point source and incorporated a ^{235}U fission energy spectra previously validated by FBR personnel. The source was collimated into a directional cone with a half-angle of 40° directed toward the armored vehicle surrogate. Shielded neutron flux was calculated using an F4 average neutron flux tally across the 12-in diameter sphere of air located in place of the largest Bonner sphere, as depicted in Fig. 3. The unshielded spectrum was simulated using the same tally and location in the absence of the vehicle surrogate. The MCNP6.1 computed neutron flux spectra for both configurations served as the *a priori* input into MAXED to assist in spectra deconvolution. Lastly, both the shielded and unshielded MCNP6.1 neutron spectra were normalized to experimental data to facilitate comparison.

Results and Analysis

Shielded Spectra Results

Fig. 4 shows the BSS-measured and MCNP6.1-simulated spectra within the armored vehicle surrogate when

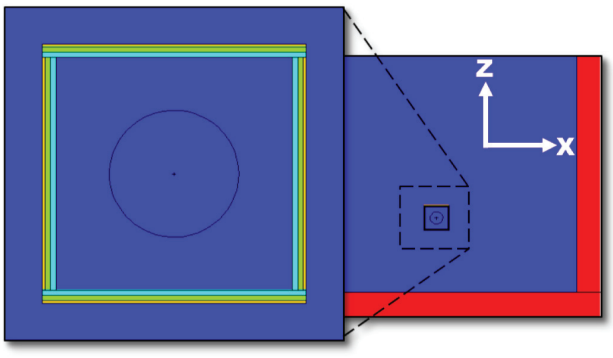

Figure 3. Horizontal view of the experiment geometry, as modeled in MCNP6.1. Dark blue represents air, while light blue is steel, green is GRP, orange is aluminum, and red is concrete.

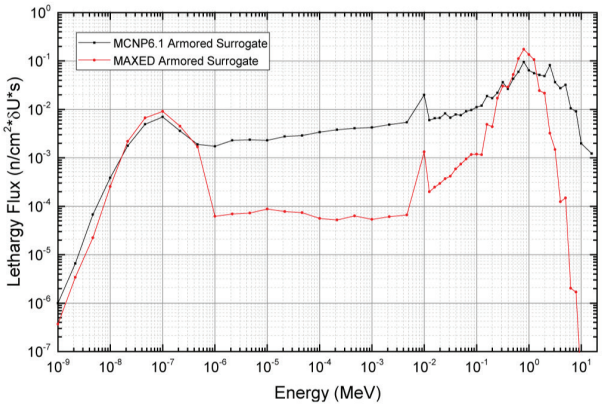

Figure 4. Neutron spectra from the ^{235}U neutron source at the WSMR FBR as measured by a BSS within the armored vehicle surrogate (red) and computed by MCNP6.1 (black) in units of lethargy flux.

exposed to the ^{235}U neutron source generated by the FBR at WSMR. The spectra demonstrate reasonable structural and intensity agreement, especially above 100 keV and across the lower energies. As anticipated, the MAXED results suffered from low resolution inherent in the BSS across intermediate energies, which is likely responsible for the disparity in intensity across that energy region. The intensity disparity above 1.1 MeV is as yet unresolved, but appears systematic due to its consistent occurrence in past studies [8].

Despite these discrepancies, the neutron spectra share a similar shape and relative intensities anticipated for a ^{235}U fission source. The MAXED solution χ^2/df-value was 0.30, which indicated the solution spectrum matched the experimental data within the measurement error tolerances to a statistically significant degree. Based upon these factors, both spectra are deemed valid approximations for the spectral neutron flux present within the armored vehicle surrogate during exposure to the FBR.

Unshielded Spectra Results

Similarly, the unshielded neutron spectra demonstrate reasonable structural and intensity agreement, specifically across energy regions above 100 keV and at the lower energies. As shown in Fig. 5 (see next page), the same BSS low-resolution effects are again present, as well as the expected peak in neutron lethargy flux for a ^{235}U fission source. Likewise, the same disparity in spectral intensity above 1.1 MeV can also be observed. Lastly, the feature occurring at 10 keV in Figs. 4 and 5 also appears

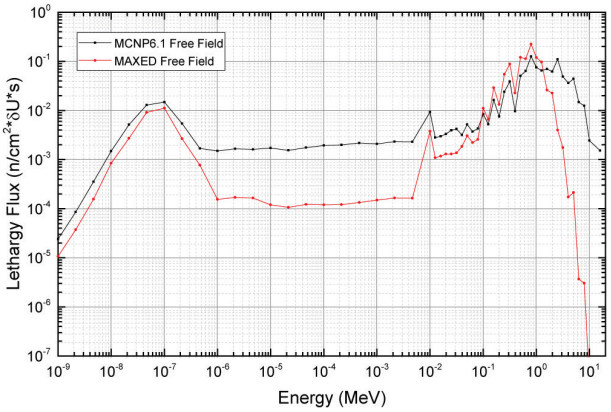

Figure 5. Neutron spectra from the ^{235}U neutron source at the WSMR FBR as measured by a BSS in the unshielded configuration (red) and computed by MCNP6.1 (black) in units of lethargy flux.

on other FBR measurements, so it is believed to be an artifact of the FBR room since it is not present in a typical watt fission spectrum.

The MAXED solution χ^2/df-value was 0.74, which indicated the solution spectrum matched the experimental data within the measurement error tolerances to a statistically significant degree. Based upon these factors, both free-field spectra are deemed valid approximations for the neutron flux present at a distance of 12 ft from the FBR.

NPF Calculation

In an effort to eliminate any additional uncertainty in the NPF calculations, neutron flux-to-dose conversion coefficients published by Veinot and Hertel [17] were applied identically to both the experimental and computational flux spectra. Using those values, ambient neutron dose equivalent *(H*(10))* totals were calculated from both shielded and unshielded MCNP6.1 and MAXED solution spectra.

For the MCNP6.1-derived neutron spectra, uncertainty propagation occurred in a straightforward manner; increasing particle tallies minimized variance and associated error. MCNP6.1 solutions passed all 10 statistical checks typically performed by MCNP to gauge tally behavior. Traditional error propagation for the experimentally measured spectra could not occur due to a lack of associated uncertainties from MAXED. Consequently, uncertainty for the MAXED solution spectra was estimated at 5% and propagated forward, which is conservative based on previous research [5], [8].

Based upon calculated *H*(10)* values, the NPF estimate provided by MCNP6.1 differed from the experimentally-derived value by ~4% relative error, as shown below in Table 1.

Table 1. Experimental and computational NPF values.

Method	NPF ± ε
Experimental (BSS and MAXED)	1.22 ± 0.06
Computational (MCNP6.1)	1.18 ± 0.02

This result is statistically significant based upon the degree of agreement and small relative uncertainties when compared to previously reported error estimates for RPFs [2]–[4]. Additionally, when compared to similar NPF research using steel shielding alone, these results indicate the new surrogate armor materials offer improved protection against neutrons [8]. These findings strongly support further research into the V&V of MCNP6.1 for RPF assessments of military vehicles.

Conclusions

Efforts remain ongoing to more explicitly identify the source of the spectral disparities between MAXED and MCNP6.1. Further analysis of neutron flux computations by MCNP6.1 still remain to be completed, and greater fidelity in the modeling of the experiment will likely minimize inconsistencies. Regardless, the V&V of MCNP6.1-generated RPF estimates for military vehicles remains ongoing, and these results further strengthen the documented accuracy and reliability of MCNP6.1 for this purpose.

Acknowledgment

The authors would like to thank the Nuclear Technologies Department of the Defense Threat Reduction Agency for their continued and ongoing support for this research.

References

[1] J.C. Nellis and J.F. Marquart, "Protection Factors of Combat Systems," *Combating WMD Journal*, vol. winter/spring, no. 8, pp. 44-46, 2012.

[2] C.R. Heimach, "Radiation Protection-Factor Measurements of a Lined Iron Box in Simulated Fission and

Fusion Tactical Nuclear Environments," Army Pulse Radiation Directorate, Aberdeen Proving Grounds, MD, 1985.

[3] C. Eisenhauer and L. Spencer, "Approximate Procedure for Calculating Protection From Initial Nuclear Radiation From Weapons," National Bureau of Standards Center for Radiation Research, Gaithersburg, 1988.

[4] C.R. Heimbach, "Final Report of Radiation Shielding in Armored Vehicles," Defense Technical Information Center, Alexandria, 1988.

[5] A.W. Decker *et al.*, "Verification and Validation of Monte Carlo N-Particle Code 6 (MCNP6) with Neutron Protection Factor Measurements of an Iron Box," *J. of Radiation Effects, Research and Engineering*, vol. 33, no.1-E, pp. 252-259, May 2015.

[6] A. Decker *et al.*, "Novel Bonner Sphere Spectrometer Response Functions Using MCNP6," *IEEE Trans. Nucl. Sci.*, vol. 62, no. 4, pp. 1689-1694, 2015.

[7] W. Erwin, "Verification and Validation of MCNP6 Using Gamma Protection Factor Measurements of an Iron Box," Air Force Institute of Technology, Dayton, 2015.

[8] A.W. Decker *et al.*, "Verification and Validation of MCNP6.1 Neutron Protection Factor Estimates Using the WSMR FBR," *J. of Radiation Effects, Research and Engineering*, vol. 35, no. 1, pp. 52-58, April 2017.

[9] T.J. Gates *et al.*, "Verification and Validation of MCNP6.1 for Gamma Protection Factor Estimates of an Armored Box," *J. of Radiation Effects, Research and Engineering*, vol. 35, no.1, pp. 83-90, April 2017.

[10] J.L. Hall *et al.*, "Verification and Validation of MCNP6.1 Gamma Protection Factor Estimates Using an Armored Box and Phantom," *J. of Radiation Effects, Research and Engineering*, vol. 35, no.1, pp. 103-110, April 2017.

[11] R.L. Bramblett *et al.*, "A New Type of Neutron Spectrometer," *Nucl. Instrument Methods*, vol. 1, p. 9, 1960.

[12] Cross Section Evaluation Working Group, Evaluated Nuclear Data File, ENDF/B-VIII.Beta4 (2017), National Nuclear Data Center, Brookhaven National Laboratory, Upton, NY, U.S.A.

[13] M. Awschalmo and R.S. Sanna, "Applications of Bonner Sphere Detectors in Neutron Field Dosimetry," U.S. Department of Energy, New York, NY, 1983.

[14] G.F. Knoll, *Radiation Detection and Measurement,* (4th ed.), Ann Arbor: John Wiley & Sons, Inc., 2010.

[15] A.V. Thomas and A.V. Alevra, "Bonner Sphere Spectrometers - A Critical Review," *Nucl. Instruments and Methods in Physics Research*, vol. A, no. 476, pp. 12-20, 2002.

[16] M. Reginatto and P. Goldhagen, "MAXED, A Computer Code for the Deconvolution of Multisphere Neutron Spectroscopy Data Using the Maximum Entropy Method," Environmental Measurements Laboratory, New York, NY, 1998.

[17] K.G. Veinot and N.E. Hertel, "Effective Quality Factors of Neutrons Based on the Revised ICRP/ICRU Recommendations," *Radiation Protection Dosimetry*, vol. 115, no. 1-4, pp. 536-541, 2005.